ACS Catalysis

LETTER

pubs.acs.org/acscatalysis

Support-Enhanced Selective Aerobic Alcohol Oxidation over Pd/Mesoporous Silicas

Christopher M. A. Parlett,[†] Duncan W. Bruce,[‡] Nicole S. Hondow,[¶] Adam F. Lee,[*,†] and Karen Wilson[†]

[†]Cardiff Catalysis Institute, School of Chemistry, Cardiff University, Cardiff CF10 3AT, U.K.

[‡]Department of Chemistry, University of York, Heslington, York YO10 5DD, U.K.

[¶]Institute for Materials Research, School of Process, Environmental and Materials Engineering, University of Leeds, Leeds, LS2 9JT, U.K.

Supporting Information

ABSTRACT: The influence of silica mesostructure upon the Pd-catalyzed selective oxidation of allylic alcohols has been investigated for amorphous and surfactant-templated SBA-15, SBA-16, and KIT-6 silicas. Significant rate enhancements can be achieved via mesopore introduction, most notably through the use of interconnected porous silica frameworks, reflecting both improved mass transport and increased palladium dispersion; catalytic activity decreases in the order Pd/KIT-6 ≈ Pd/SBA-16 > Pd/SBA-15 > Pd/SiO_2. Evidence is presented that highly dispersed palladium oxide nanoparticles, not zerovalent palladium, are the catalytically active species.

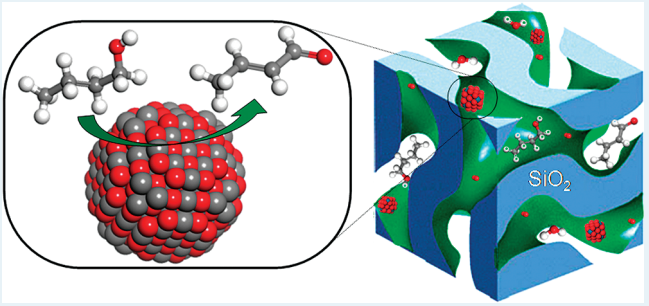

KEYWORDS: Palladium, alcohol, selective oxidation, mesoporous, silica, active site

INTRODUCTION

Selective aerobic oxidation of alcohols represents an elegant class of atom-efficient molecular transformations for chemical valorization, that are catalyzed under mild conditions by a range of supported or colloidal platinum-group and noble-metal nanoparticles.[1] For primary alcohols, the desired products are valuable intermediates for the fine chemical, pharmaceutical, and agrochemical sectors with allylic aldehydes in particular, high-value components for the perfume, and flavorings industries;[2] crotonaldehyde is an termite repellant and precursor to the food preservative sorbic acid, while cinnamaldehyde confers a cinnamon flavor and aroma. The most promising heterogeneous catalysts derive from nanocrystalline Au,[3] Pd,[4,5] and bimetallic formulations thereof,[6] typically dispersed on high-area carbon[7] or oxide supports,[6,8] wherein rate/selectivity improvements have proceeded largely via empirical approaches. While these have uncovered, for example, interesting synergies between Au and Pd, and differences between carbon versus oxide supports, the design and optimization of such catalysts remains hampered by a limited understanding of the active site responsible for the (rate-limiting) oxidative dehydrogenation step[9−11]

Recently, we showed that high surface area (300 m^2g^{-1}), mesoporous alumina was able to stabilize atomically dispersed Pd^{II} centers that exhibit exceptional activity toward the aerobic selective oxidation (selox) of allylic alcohols.[5] However, it is unclear to what extent our observation that electron-deficient palladium is the active species in catalyzing oxidative dehydrogenation can be generalized to related (and especially nonreducible) oxide supports; similar Pd^{II} species have been noted on stoichiometric hydroxyapatite but are proposed merely as precursors to active metallic nanoclusters formed in situ during alcohol selox. Furthermore, although a range of support materials[8,12,13] have been employed by different groups to disperse typically high (>1 wt %) loadings of Pd nanoparticles, nothing is known regarding the influence of support architecture upon the resulting reactivity. The vast majority of such selective alcohol oxidations are conducted in the liquid phase, many utilizing relatively bulky substrates, hence the latter is an important consideration since the introduction of macro- or mesopores can strongly affect mass transport to in-pore active sites.[14,15]

RESULTS AND DISCUSSION

To address the preceding questions, we synthesized systematically and studied four related families of Pd/SiO_2 catalysts with similar metal loadings spanning 0.05−4 wt % Pd: a commercial, low-area SiO_2 (200 $m^2\ g^{-1}$); SBA-15, a high surface area supports with hexagonally packed, p6mm, parallel mesopore channels (950 $m^2\ g^{-1}$); and two high surface area cubic silica supports with three-dimensional interpenetrating mesopore networks, SBA-16, Im3m, (820 $m^2\ g^{-1}$) and KIT-6, Ia3d, (940 $m^2\ g^{-1}$), potentially linked via micropores.

Mesoporous silicas offer several advantages over their alumina counterparts such as reproducible and scalable synthesis, significantly

Received: March 15, 2011
Revised: May 1, 2011
Published: May 03, 2011

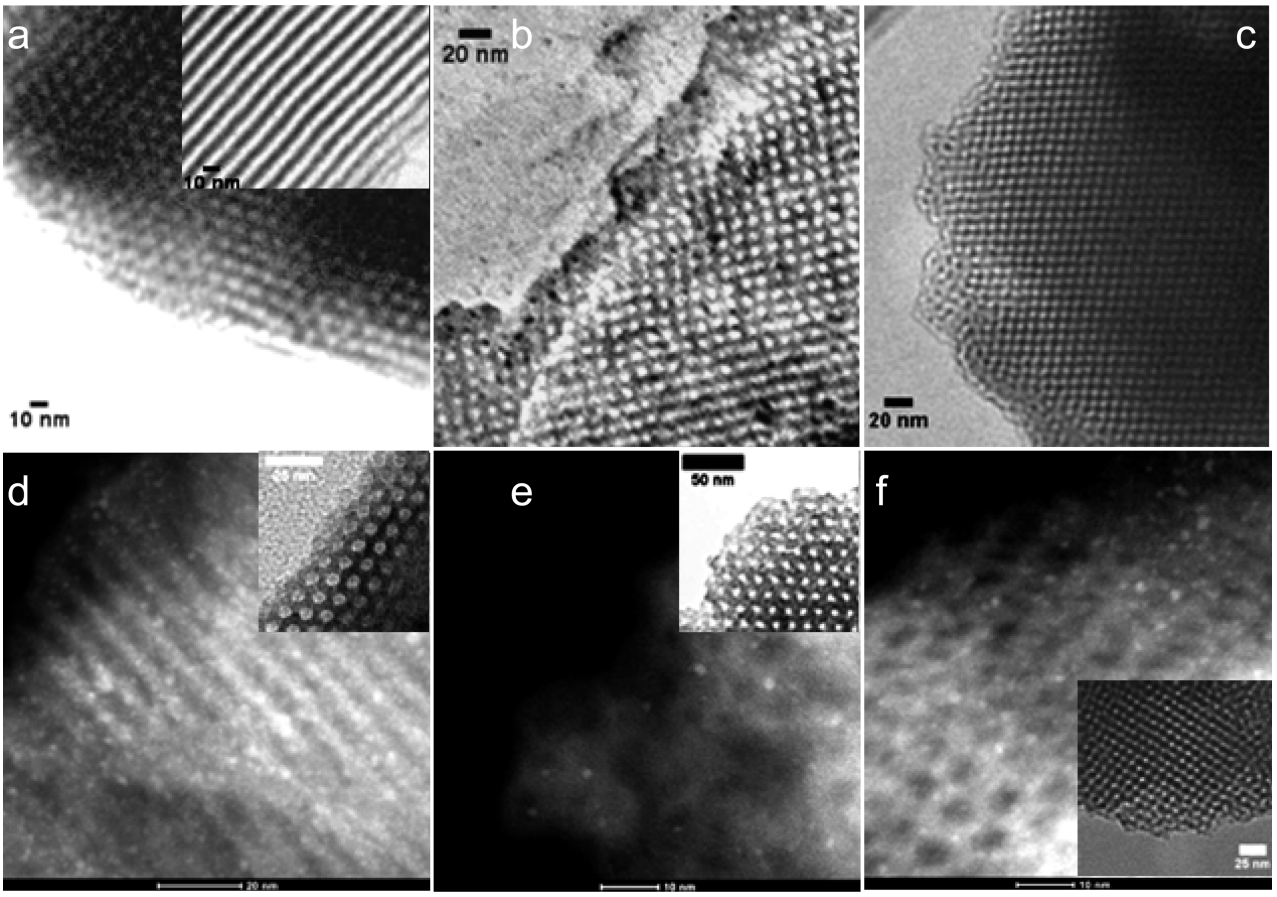

Figure 1. High-resolution TEM (HRTEM) bright-field images of parent (a) SBA-15, (b) SBA-16, and (c) KIT-6 supports, and HAADF-STEM images of (d) 1 wt % Pd/SBA-15, (e) 1 wt % Pd/SBA-16, and (f) 1 wt %/KIT-6 catalysts, highlighting Pd nanoparticles dispersed throughout mesopore networks (bright spots); insets show bright-field HRTEM images of parent SBA-15 and Pd-impregnated mesoporous silicas.

higher surface areas and more flexible pore architectures;[16,17] some silicas possessing interconnected mesopore networks that enhance molecular diffusion and even favor different dispersed species.[18,19] Indeed, a three-dimensional, spongelike organosilane-functionalized TUD-1 mesoporous silica was recently shown to outperform MCM-41 in Pd-catalyzed benzyl alcohol selox.[20] Successful synthesis of our three mesoporous supports, SBA-15, SBA-16, and KIT-6, and associated Pd incorporation within their pore networks was confirmed by porosimetry, powder X-ray diffraction (XRD), and transmission electron microscopy (TEM) (Figure 1 and Supporting Information S1−13). Textural properties of the resulting Pd-impregnated materials are summarized in Supporting Information Tables S1−2, and are in accordance with literature values for the parent silicas.[8] All samples exhibited Type IV adsorption isotherms with Type I (SBA-15 and KIT-6) or II (SBA-16) hysteresis (Supporting Information Figures S6−8). XRD and porosimetry reveal no significant change in either mesopore unit cell or pore diameters following Pd incorporation, while Brunauer−Emmett−Teller surface areas and pore volumes decrease with metal loading by 30−40% for the mesostructured silicas, consistent with pore blockage (Supporting Information Table S2).[16,17] The amorphous support exhibits a proportionally smaller loss in surface area, indicative of larger nanoparticles and predominant decoration of the external surface of silica particles.

As expected, metal dispersions determined by CO chemisorption show an inverse correlation with Pd loading; corresponding particle sizes (confirmed by TEM and wide-angle XRD for loadings >3 wt %) exhibit a pronounced increase from ∼1 nm (0.05 wt %) to 4 nm (4.1 wt %). These trends are mirrored by the palladium surface oxidation state, which is a strong function of both metal loading and support structure (Supporting Information Figure S14−15 and Table S2). In accordance with Pd/C and Pd/Al_2O_3 systems, surface oxidation increases substantially below 1 wt % Pd but also increases from SiO_2 < SBA-15 < SBA-16 ≈ KIT-6; this has a major impact on the resulting selox performance.

The catalytic performance of all four Pd/SiO_2 series was first evaluated toward the aerobic selox of crotyl (CrOH) and cinnamyl (CinnOH) alcohols to their corresponding allylic aldehydes. In order to ensure that intrinsic reaction kinetics were measured across these silica families (spanning a wide range of surface area and porosity), their differing mass transport properties were assessed by studying the effect of mixing upon initial rates (Figure 2a,b). Introducing mesopore interconnectivity improved mass transport for both alcohols (evidenced by a plateau in activity attained at lower stirrer speeds for SBA-16/KIT-6 versus SBA-15) with KIT-6 proving slightly superior to SBA-16 for the larger alcohol, something we attribute to the narrower "ink bottle" pore openings of the latter.[16] Hot-filtration experiments (Supporting Information Figure S17) and elemental analysis on both filtrate and spent catalysts (Supporting Information Figure S18 and Table S3) revealed no evidence of Pd leaching.

dx.doi.org/10.1021/cs200145n |*ACS Catal.* 2011, 1, 636–640

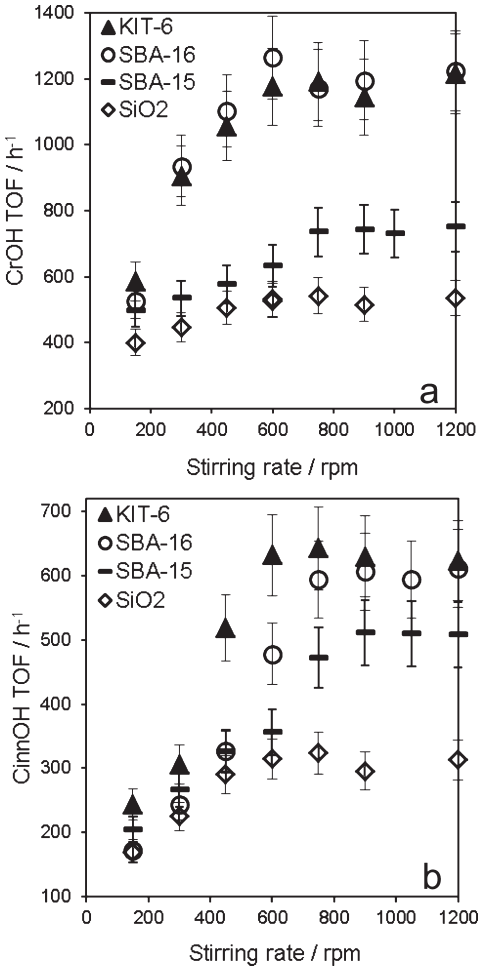

Figure 2. Effect of stirring rate on turnover frequency (TOF) toward (a) CrOH and (b) CinnOH aerobic selox of 1 wt % Pd 2.5 wt % Pd/silicas, respectively. All reactions conducted at 90 °C with 50 mg of catalyst and 8.4 mmol of alcohol.

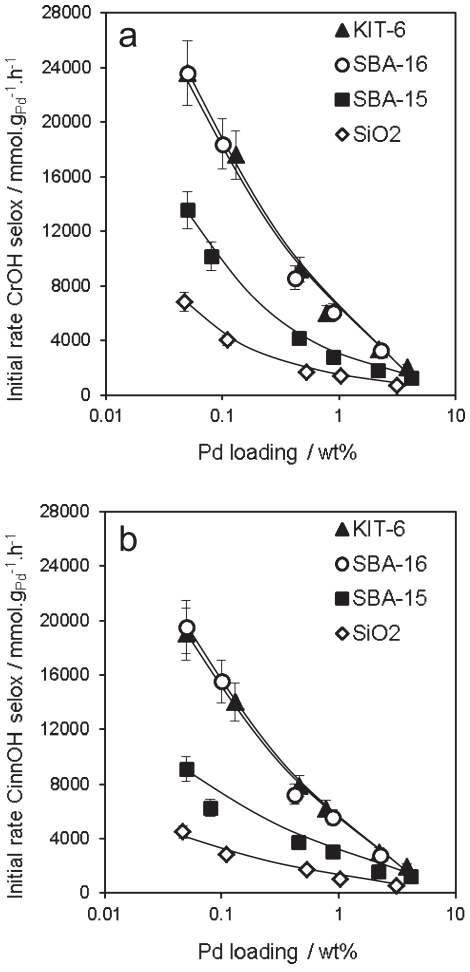

Figure 3. Rate dependence of (a) crotyl and (b) cinnamyl alcohol aerobic selox on bulk Pd loading and silica support.

Operation under nonmass transfer limited conditions at high stirrer rates was confirmed by varying the catalyst/substrate ratio and oxygen flow rate (Supporting Information Figure S16) and reveals that initial selox rates for CrOH and CinnOH alcohol selox are inversely proportional to Pd loading for all silicas (Figure 3a,b), which is in accordance with our observations for Pd-impregnated aluminas,[5,9,21,22] indicating pronounced particle size effects. One should note that while the absolute rise in particle sizes with loading are comparatively small across the 0.05−1 wt % range in Supporting Information Table S2, all four catalyst families exhibit systematic size increases over precisely this regime in which electronic and geometric properties of nanoparticles evolve most rapidly. For example, Pd paricles in the SBA-15 family increase from <1 to 2.3 nm as the Pd loading rises from 0.05 to 0.89 wt %. In the case of spherical morphologies, this apparently small increase in cluster diameter would expand individual clusters from only 43 to 429 total Pd atoms, while the fraction of the most reactive, low-coordinate Pd atoms (≤6 nearest neighbors) falls from 55 to 11%. Such geometric changes and surface energetics are expected to strongly favor Pd oxide formation over the smaller particles, versus Pd metal above 2 nm. Activity increases associated with falling Pd loadings are also a strong function of the support, rising disproportionately in the order SiO_2 < SBA-15 < SBA-16 ≈ KIT-6. The superior activity of all the mesoporous supports over commercial silica can be attributed to their higher Pd dispersions. However, despite their similar surface areas and pore diameters, an additional rate enhancement is observed upon switching from the parallel, noninterconnected channels within SBA-15, to the interconnected pore networks of SBA-16 and KIT-6, consistent with the latters' ability to stabilize even more highly dispersed Pd nanoparticles.

Having observed a direct relationship between Pd dispersion and selox activity, the question arises as to the nature of the active palladium species. Simple comparison of the initial rate dependence of CrOH or CinnOH selox versus the surface PdO concentration within as-prepared Pd/silicas shown in Figure 4 immediately suggests surface oxide as a likely active site. However, since it is known that PdO can undergo in situ reduction to Pd^0 during alcohol selox, the relationship in Figure 4 could merely reflect the surface oxide concentration in fresh catalysts providing a predictor for the subsequent concentration of active metal sites generated under reaction conditions; more sophisticated analysis of TOFs versus oxide or metal content (independently quantified) is necessary.

If a single active site is responsible for selox at both low and high Pd loadings, and the trends in Figure 3a,b simply reflect changes in the number of such sites (i.e., selox is structure insensitive), then normalizing these initial rates to the site density should result in a constant (nanoparticle size/Pd-loading

dx.doi.org/10.1021/cs200145n |ACS Catal. 2011, 1, 636–640

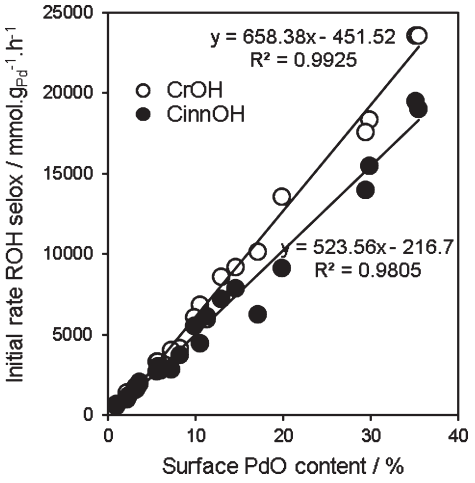

Figure 4. Linear relationship between CrOH and CinnOH aerobic selox rates over Pd/silicas and surface PdO content determined by XPS. Data is composite of all results from SiO_2, SBA-15, SBA-16, and KIT-6 silica families.

independent) turnover frequency. In contrast, if the resulting turnover frequencies are themselves a function of nanoparticle size/Pd loading (i.e., selox is structure sensitive), then either multiple active sites exist with differing kinetics, or the true, single, active species has not been identified correctly. Literature models for Pd-catalyzed allylic alcohol selox are dominated by two candidate active species, metallic (Pd^0)[23] or surface PdO_x[5,9] (wherein Pd^{II} is proposed, irrespective whether the oxide is stoichiometric or substoichiometric). Therefore, we tested both models against our combined body of data for all four Pd/silica families in order to elucidate the active site. Figure 5a,b shows the resulting turnover frequencies, normalized either to the number of metal surface atoms (from CO chemisorption) or Pd^{II} surface atoms (from XPS), as a function of each palladium species.

The outcome is striking. Normalization to PdO yields a constant turnover frequency of ~7000 (~5000) h^{-1} for CrOH (CinnOH), independent of either metal loading or support properties; in contrast, normalization to metallic Pd reveals a strong structure sensitivity. This (i) provides unequivocal evidence that Pd^0 cannot be the sole active species responsible for selox and (ii) points overwhelmingly toward surface PdO as the active site. The latter conclusion is further supported by a quantitative comparison of the TOFs derived in Figure 5 (per Pd^{2+} site) against those obtained for atomically dispersed Pd^{II} centers on alumina of 7080 h^{-1} for CrOH and 4400 h^{-1} for CinnOH. The similarity of these values to those observed herein over four different silica supports indicates that an intrinsic rate, characteristic of a common surface PdO active species, has indeed been determined. These findings are in excellent agreement with our recent DRIFTS/MS/XAS study of vapor phase, crotyl alcohol selox over nanoparticulate Pd,[24] wherein in situ measurements revealed Pd^{2+} and not Pd metal promoted oxidative dehydrogenation to crotonaldehyde. We have screened our Pd/mesporous silica catalysts against a range of substrates and have observed similar behavior toward crotyl/cinnamyl alcohols as for diverse primary and secondary allylic alcohols (Supporting Information Table S4), highlighting the general significance of our findings for the design of future Pd allylic alcohol selox catalysts.

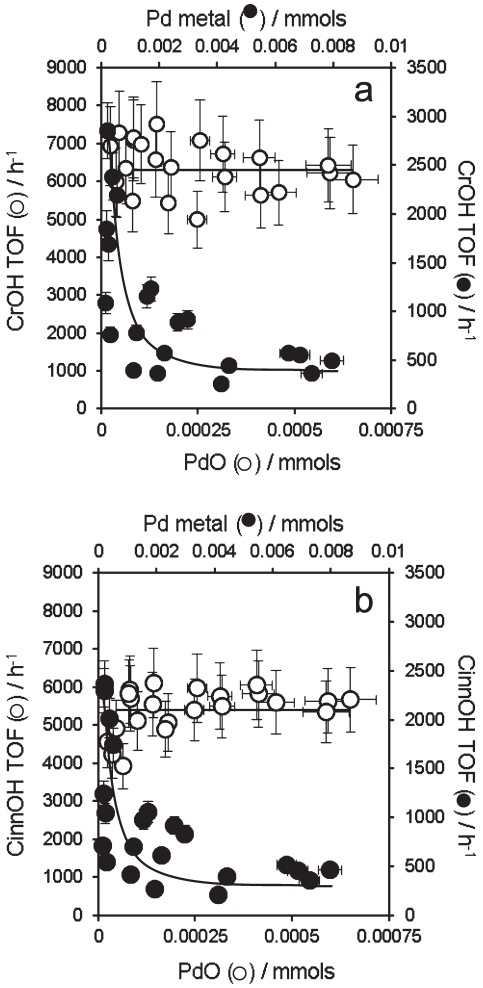

Figure 5. (a) Crotyl and (b) cinnamyl alcohol aerobic selox turnover frequencies as a function of surface PdO or Pd metal content for Pd/SiO_2, Pd/SBA-15, Pd/SBA-16, and Pd/KIT-6 catalysts. Bulk Pd loadings span 0.05−4.2 wt %.

In conclusion, four series of related Pd/silica catalysts have been synthesized, all of which are active for allylic alcohol selox under mild conditions. Varying the support architecture, in particular the introduction of interconnected mesopore networks, enables tuning of both mass-transport characteristics and Pd dispersion with SBA-16 and KIT-6 both exhibiting enhanced performance over SBA-15; the narrower pore openings of SBA-16 may hinder diffusion of bulkier alcohols compared with KIT-6.[25] Initial selox rates are proportional to Pd dispersion and surface PdO concentration, the latter increasing significantly for mesoporous silicas, notably interconnected SBA-16/KIT-6. Crotyl and cinnamyl alcohol turnover frequencies determined across all four Pd/silicas provide strong evidence that surface PdO, not Pd metal, is the active species in allylic alcohol selox over oxide-supported Pd nanoparticles.

■ ASSOCIATED CONTENT

Supporting Information. Full catalyst synthesis and characterization, reaction conditions, and selox results for additional alcohol substrates. This material is available free of charge via the Internet at http://pubs.acs.org.

dx.doi.org/10.1021/cs200145n |ACS Catal. 2011, 1, 636–640

AUTHOR INFORMATION

Corresponding Author
*E-mail: leeaf@cardiff.ac.uk.

ACKNOWLEDGMENT

We thank the EPSRC (EP/E046754/1; EP/G007594/2) for financial support, a Leadership Fellowship (A.F.L.), and studentship support (C.M.A.P.), and the ESRF for beamtime (CH2432). Electron microscopy access was provided through the Leeds EPSRC Nanoscience and Nanotechnology Research Equipment Facility (LENNF) (EP/F056311/1).

REFERENCES

(1) Vinod, C. P.; Wilson, K.; Lee, A. F. *J. Chem. Technol. Biotechnol.* **2011**, *86*, 161–171.
(2) Uozumi, Y.; Yamada, Y. M. A. *Chem. Rec.* **2009**, *9*, 51–65.
(3) Della Pina, C.; Falletta, E.; Prati, L.; Rossi, M. *Chem. Soc. Rev.* **2008**, *37*, 2077–2095.
(4) Mori, K.; Hara, T.; Mizugaki, T.; Ebitani, K.; Kaneda, K. *J. Am. Chem. Soc.* **2004**, *126*, 10657–10666.
(5) Hackett, S. E. J.; Brydson, R. M.; Gass, M. H.; Harvey, I.; Newman, A. D.; Wilson, K.; Lee, A. F. *Angew. Chem., Int. Ed.* **2007**, *46*, 8593–8596.
(6) Enache, D. I.; Edwards, J. K.; Landon, P.; Solsona-Espriu, B.; Carley, A. F.; Herzing, A. A.; Watanabe, M.; Kiely, C. J.; Knight, D. W.; Hutchings, G. J. *Science* **2006**, *311*, 362–365.
(7) Bianchi, C. L.; Biella, S.; Gervasini, A.; Prati, L.; Rossi, M. *Catal. Lett.* **2003**, *85*, 91–96.
(8) Li, C. L.; Zhang, Q. H.; Wang, Y.; Wan, H. L. *Catal. Lett.* **2008**, *120*, 126–136.
(9) Lee, A. F.; Hackett, S. F. J.; Hargreaves, J. S. J.; Wilson, K. *Green Chem.* **2006**, *8*, 549–555.
(10) Grunwaldt, J. D.; Caravati, M.; Baiker, A. *J. Phys. Chem. B* **2006**, *110*, 25586–25589.
(11) Keresszegi, C.; Burgi, T.; Mallat, T.; Baiker, A. *J. Catal.* **2002**, *211*, 244–251.
(12) Karimi, B.; Zamani, A.; Abedia, S.; Clark, J. H. *Green Chem.* **2009**, *11*, 109–119.
(13) Chen, J.; Zhang, Q. H.; Wang, Y.; Wan, H. L. *Adv. Synth. Catal.* **2008**, *350*, 453–464.
(14) Dacquin, J. P.; Cross, H. E.; Brown, D. R.; Duren, T.; Williams, J. J.; Lee, A. F.; Wilson, K. *Green Chem.* **2010**, *12*, 1383–1391.
(15) Dhainaut, J.; Dacquin, J. P.; Lee, A. F.; Wilson, K. *Green Chem.* **2010**, *12*, 296–303.
(16) Zhao, D. Y.; Feng, J. L.; Huo, Q. S.; Melosh, N.; Fredrickson, G. H.; Chmelka, B. F.; Stucky, G. D. *Science* **1998**, *279*, 548–552.
(17) Kleitz, F.; Choi, S. H.; Ryoo, R. *Chem. Commun.* **2003**, 2136–2137.
(18) Tsoncheva, T.; Ivanova, L.; Rosenholm, J.; Linden, M. *Appl. Catal., B* **2009**, *89*, 365–374.
(19) Soni, K.; Mouli, K. C.; Dalai, A. K.; Adjaye, J. *Catal. Lett.* **2010**, *136*, 116–125.
(20) Chen, Y.; Guo, Z.; Chen, T.; Yang, Y. *J. Catal.* **2010**, *275*, 11–24.
(21) Lee, A. F.; Wilson, K. *Green Chem.* **2004**, *6*, 37–42.
(22) Chen, Y. T.; Lim, H. M.; Tang, Q. H.; Gao, Y. T.; Sun, T.; Yan, Q. Y.; Yang, Y. H. *Appl. Catal., A* **2010**, *380*, 55–65.
(23) Grunwaldt, J. D.; Caravati, M.; Baiker, A. *J. Phys. Chem. B* **2006**, *110*, 25586–25589.
(24) Lee, A. F.; Ellis, C. V.; Naughton, J. N.; Newton, M. A.; Parlett, C. M. A.; Wilson, K. *J. Am. Chem. Soc.* **2011**, *133*, 5724–5727.
(25) Huirache-Acuna, R.; Pawelec, B.; Rivera-Munoz, E.; Nava, R.; Espino, J.; Fierro, J. L. G. *Appl. Catal., B* **2009**, *92*, 168–184.